IIETA International Information and Engineering Technology Association
Advancing the World of Information and Engineering

Mathematical Modelling of Engineering Problems
Vol. 13, No. 4, April, 2026, pp. 621-632
Journal homepage: http://iieta.org/journals/mmep

Numerical Design Methodology for Resistor–Capacitor Phase-Shift Oscillators with Accurate Frequency Targeting

Muhannad Al-Tarifi[1*], Sameer Arabasi[2], Dima Bader[1], Moussa Habib[1]

[1] Department of Electrical Engineering, Al Hussein Technical University, Amman 11831, Jordan
[2] Department of Basic Sciences, German Jordanian University, Amman 11180, Jordan

Corresponding Author Email: Muhannad.Altarifi@htu.edu.jo

https://doi.org/10.18280/mmep.130401

Received: 6 February 2026
Revised: 14 April 2026
Accepted: 23 April 2026
Available online: 15 May 2026

Keywords:
Resistor–Capacitor phase-shift oscillators, operational amplifiers, feedback design, numerical analysis, harmonic distortion, transfer function, frequency control

ABSTRACT

This paper presents a numerical methodology for designing Resistor–Capacitor (RC) phase-shift oscillators that reliably achieve the target frequency without post-design tuning. RC phase-shift oscillators, composed of cascaded RC networks and a single operational amplifier (op-amp), are widely used for low-cost, compact sinusoidal signal generation. Conventional design approaches often assume ideal op-amp behavior and neglect loading effects from finite input impedance, leading to deviations between expected and actual performance. Even advanced models that account for loading typically provide only critical oscillation conditions, requiring post-design adjustment to achieve the desired frequency. In contrast, the proposed method employs numerically generated design curves for forward gain values exceeding critical thresholds, derived from feedback control modeling. This approach ensures oscillation initiation and eliminates the need for post-design tuning. Design cases including multiple 3-stage and 4-stage oscillators demonstrate frequency accuracy within ±0.5%. Validation through simulations and prototype measurements confirms the methodology's reliability. The approach is generalizable to other oscillator types, supporting flexible component selection, reduced harmonic distortion, and precise frequency control.

1. INTRODUCTION

Single operational-amplifier (op-amp) resistor–capacitor (RC) phase-shift oscillators are widely used because of their simplicity and low cost. This type of oscillator has found widespread applications across several fields due to its low component count and ease of integration. To mention a few, they are used in tone generators, synthesizers, and function generators. The low distortion and frequency stability provided by a carefully tuned RC phase-shift oscillator make it ideal for generating pure sine waves. They also serve as reliable signal sources for calibrating and testing electronic circuits. The compact nature and minimal power requirements of single op-amp designs make them attractive for use in portable and battery-powered systems. They also have myriad applications in communication systems and education [1-8].

In these circuits, also called RC ladder oscillators, a single op-amp is combined with a cascade of RC networks as feedback to create the frequency-dependent phase shift necessary for sustained oscillations. Typically, in a three-stage RC network, each RC section is ideally designed to contribute 60° of phase shift. Together with the inherent 180° phase inversion provided by the op-amp, the network reaches the 360° required for positive feedback and continuous oscillation.

Early investigations into oscillator design also drew on impedance-matching and terminating-impedance viewpoints [9-16]. These works provided foundational insight into RC-network loss, oscillation requirements, and related design limits. Other studies later derived analytical expressions and practical design equations for three- and four-section phase-shift networks under specific circuit assumptions [17, 18]. The present work does not claim that the broader matching literature neglected loading in general. Rather, the focus here is on a practical single op-amp RC phase-shift design process in which the amplifier input resistance is incorporated explicitly, and in which operation beyond the critical condition is used to predict the realized oscillation frequency more directly and reduce the need for after-design tuning.

More recent studies have revisited the fundamental oscillation conditions by comparing the classical Barkhausen criterion with the Nyquist stability approach [19-24]. Their analysis reveals that while the Barkhausen criterion offers necessary conditions for oscillation, it falls short in predicting startup behavior, particularly when the gain surpasses the critical oscillation threshold. It is concluded that the typical formulations are incomplete and insufficient for a comprehensive design, thus reinforcing the need for an improved methodology [21].

General oscillation conditions were introduced, utilizing the Routh-Hurwitz stability criterion to determine the oscillation startup conditions and frequencies [24-26]. This method provides a systematic approach, contrasting with the Barkhausen criterion that focuses solely on loop gain. Instead, this general method examines the characteristic equation of the

reduced transfer function of the oscillator's feedback system. This precise representation enables the identification of pole behavior at critical stability and allows for the numerical evaluation of oscillation frequencies beyond the critical condition [24]. In parallel, recent studies indicate continuing development in RC and related sinusoidal oscillator design, including nonlinear Hopf-bifurcation analysis of op-amp RC phase-shift oscillators, amplifier-based oscillator synthesis, tunable-phase third-order oscillators, and independently tunable active-RC oscillator structures [27-31]. Despite these advantages, there remains a lack of published work that effectively applies this technique to develop a straightforward yet rigorous design process that accurately accounts for the real oscillation frequency, which often deviates from the predicted critical frequency.

In this paper, we introduce a step-by-step design process tailored for crafting RC phase shift oscillators that operate with precision in practical scenarios. This process begins with a specific oscillation frequency required by the application, called the design (or target) frequency. To support this process, we have created detailed design curves that map out the frequency alongside the forward gain. These numerically developed curves serve as a comprehensive resource for designers, enabling the rapid selection and assembly of circuit components. This approach ensures that the oscillator will achieve oscillation at the desired frequency with a high degree of accuracy (within ±0.5%).

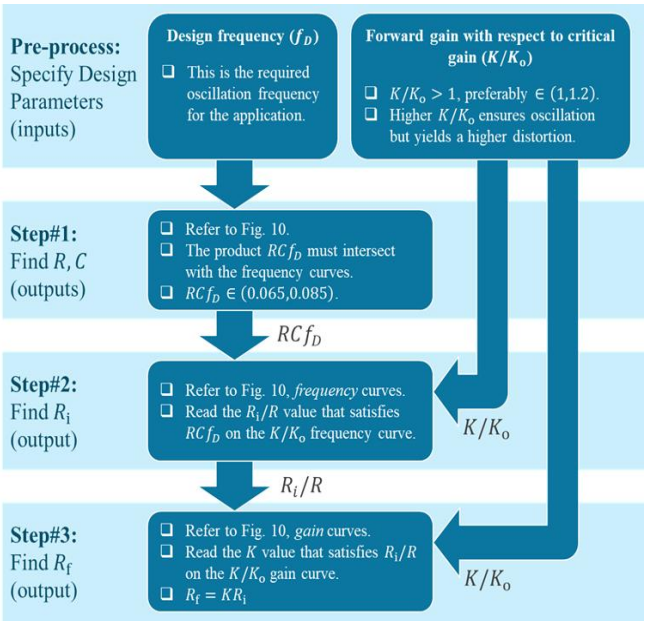

Figure 1. Proposed 3-step process to design a single op-amp Resistor–Capacitor (RC) phase-shift oscillator with high practical accuracy and no after-design tuning

Note: The specific range of RCf_D in step#1 is tailored for the 3-stage configuration.

Figure 1 provides a summary of the design process we have outlined. Beginning with the required oscillation frequency (i.e., design frequency), the designer can follow a three-step sequence to identify all necessary components of the oscillator. This process is predicated on selecting a forward gain that exceeds the critical gain from the outset, thereby ensuring oscillation startup in practical applications. However, when a higher forward gain is required, the traditional formulas for critical gain and frequency become inapplicable, necessitating a numerical approach. This numerical problem is uniquely addressed by reversing the typical sequence: starting with the required frequency and working backwards to deduce the oscillator component values. Our numerically developed design curves are instrumental in this reversed process. As a result, the heavy after-design tuning required in conventional approaches, i.e., post-design adjustment of component values to initiate oscillation or bring the oscillation frequency closer to the target, is rarely necessary. This work proposes a practical design process that incorporates the prediction of oscillator behavior beyond critical conditions, especially for forward gains exceeding the critical gain.

We initiate our analysis with a configuration of the 3-stage RC oscillator (CR-CR-CR) utilizing a single op-amp. By applying control theory principles of feedback systems, we develop the overall transfer function, identifying the critical stability gain condition and the corresponding critical frequency. We then discuss the practical challenges of initiating oscillation with these explicit formulas that necessitate extensive after-design tuning, highlighting the limitations of conventional approaches. Consequently, we detail the numerical development of gain-frequency relations beyond critical stability (i.e., forcing some degree of instability), as explicit formulas are inadequate when the forward gain exceeds the critical threshold. The effectiveness and precision of the numerically derived design curves are demonstrated through a step-by-step process, validated by multiple examples with support from Multisim simulations and a measured prototype. This methodology is similarly applied to another 3-stage configuration (RC-RC-RC) and two 4-stage configurations (CR-CR-CR-CR and RC-RC-RC-RC), with design curves for each configuration displayed and validated.

2. MODELING 3-STAGE LADDER OSCILLATOR

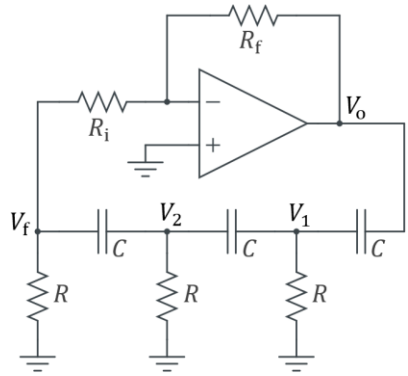

Figure 2. Three-stage, single op-amp, Resistor–Capacitor (RC) phase-shift oscillator

Note: The ladder arrangement is CR-CR-CR type, denoting the order of ladder components starting from the op-amp output node (at V_o) and ending at its input node (at V_f).

The circuit under detailed investigation in this paper is shown in Figure 2. The circuit comprises a single op-amp with a feedback network consisting of three identical RC stages, configured in a CR-CR-CR arrangement. This configuration begins with a capacitor connected to the op-amp's output (with output voltage, V_{out}), followed by a shunt resistor at its other terminal (with voltage V_1). This arrangement is repeated across each stage until the third shunt resistor at the final node of the feedback ladder (with feedback voltage, V_f). The feedback voltage then feeds the inverting op-amp circuit that

amplifies it with a gain equal to the ratio of the feedback and input impedances (in this case, both impedances are resistors). This section first formulates the oscillation conditions and then validates them through simulations in Simulink and Multisim.

It is important to note that the formulation and characterization methods described for this circuit are broadly applicable to various RC ladder configurations, which may include different numbers of stages (e.g., four stages) or alternate arrangements (e.g., RC-RC-RC type). Further discussion of this adaptability is provided in Section 5.

2.1 Explicit formulas for critical oscillation conditions

Analysis begins by formulating the transfer functions for both the forward and feedback paths. The forward path is defined as the ratio of the op-amp output voltage (V_o) to the input voltage (V_f) through the inverting amplifier stage, with its transfer function presented as:

$$G = \frac{V_\mathrm{o}}{V_\mathrm{f}} = \frac{-R_\mathrm{f}}{R_\mathrm{i}} = -K \tag{1}$$

where, $K = R_\mathrm{f}/R_\mathrm{i}$ is a positive number representing the absolute value of the forward gain. Conversely, the feedback path's transfer function is the ratio of the ladder input voltage (V_o) to the ladder output voltage (V_f), calculated through a 3-stage RC ladder circuit. Application of nodal analysis to nodes V_1, V_2, and V_f yields the following equations:

$$sC(V_1 - V_2) + \frac{1}{R}V_1 + sC(V_1 - V_\mathrm{o}) = 0 \tag{2}$$

$$sC(V_2 - V_\mathrm{f}) + \frac{1}{R}V_2 + sC(V_2 - V_1) = 0 \tag{3}$$

$$sC(V_\mathrm{f} - V_2) + \frac{1}{R}V_\mathrm{f} + \frac{1}{R_\mathrm{i}}V_\mathrm{f} = 0 \tag{4}$$

These equations include the resistor (R_i), factoring in the loading effect this resistor has on the ladder's operation. Solving these equations provides the feedback path's transfer function:

$$H = \frac{V_\mathrm{f}}{V_\mathrm{o}} = \frac{\mathrm{Num}\{H\}}{\mathrm{Den}\{H\}} \tag{5}$$

where,

$$\mathrm{Num}\{H\} = C^3R^3\frac{R_\mathrm{i}}{R}s^3,$$

$$\mathrm{Den}\{H\} = C^3R^3\frac{R_\mathrm{i}}{R}s^3 + \left(3 + 6\frac{R_\mathrm{i}}{R}\right)C^2R^2s^2 + \left(4 + 5\frac{R_\mathrm{i}}{R}\right)CRs + \left(\frac{R_\mathrm{i}}{R} + 1\right).$$

Both transfer function blocks incorporate the loading effect, allowing the typical control theory of feedback systems to be applied. This formulation allows for the application of feedback control principles, which involve considering the effects of disturbances, such as noise or pulse inputs, at the V_f node. Consequently, the overall system transfer function can be expressed as G/(1-GH), with the characteristic equation:

$$(1 + K)C^3R^3\frac{R_\mathrm{i}}{R}s^3 + \left(3 + 6\frac{R_\mathrm{i}}{R}\right)C^2R^2s^2 + \left(4 + 5\frac{R_\mathrm{i}}{R}\right)CRs + \left(\frac{R_\mathrm{i}}{R} + 1\right) = 0 \tag{6}$$

The roots of this equation (i.e., the system's poles) determine stability and oscillation frequency. For oscillator applications, instability is desirable, achieved when the real part of at least one pole is positive. At critical stability, the real part of the pole is zero. By rewriting Eq. (6) in the standard cubic form and applying the Routh-Hurwitz criterion, the oscillation boundary can be obtained directly. The intermediate derivation steps are provided in Appendix A, which yields the following explicit formula for the minimum forward-path gain K_o (critical gain):

$$K_\mathrm{o} = \frac{29\left(\frac{R_\mathrm{i}}{R}\right)^2 + 38\frac{R_\mathrm{i}}{R} + 12}{\left(\frac{R_\mathrm{i}}{R}\right)^2 + \frac{R_\mathrm{i}}{R}} \tag{7}$$

Furthermore, the oscillation frequency under critical conditions (f_o) can be explicitly formulated from the imaginary part of the related pole, and can be expressed as:

$$f_\mathrm{o} = \frac{1}{2\pi\sqrt{3}RC}\sqrt{\frac{1 + R_\mathrm{i}/R}{1 + 2\,R_\mathrm{i}/R}} \tag{8}$$

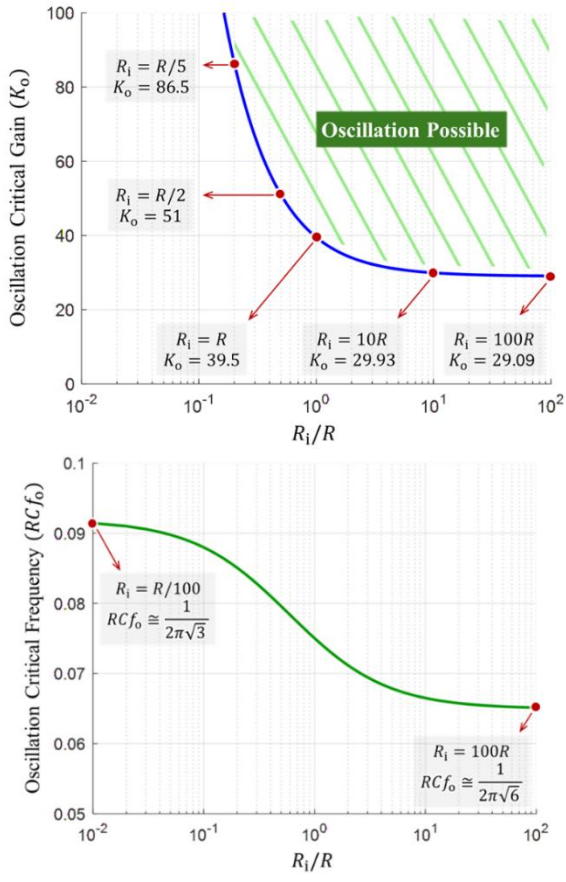

Figure 3. Oscillation critical gain (top) and oscillation critical frequency (bottom) of the Resistor–Capacitor (RC) ladder oscillator in Figure 2 versus the ratio R_i/R
Note: Both curves are based on the explicit Eqs. (7) and (8).

Figure 3 illustrates the critical gain and critical frequency curves as the ratio R_i/R varies from 0.01 to 100. Several key observations can be made from these curves. First, when the input resistance is very high relative to R, the amplifier imposes only weak loading on the RC ladder, and the classical results are recovered: the critical gain approaches 29, and the

critical frequency approaches $1/(2\pi RC\sqrt{6})$. Second, as R_i approaches the magnitude of R (e.g., $R_i = R$), the loading effect becomes significant, which alters both the attenuation and the phase behavior of the ladder. As a result, the critical gain increases appreciably above 29 (e.g., $K_o = 39.5$ when $R_i = R$), and the oscillation frequency shifts by about 10–20%. This explains why conventional design approaches that do not explicitly account for loading can lead to noticeable frequency error and require substantial after-design tuning.

When the ratio R_i/R becomes small, the loading effect becomes severe, and the gain required for oscillation onset rises rapidly, becoming impractically high when R_i is less than one fifth of R. From a design perspective, the selection of ladder resistor and capacitor values (R and C) is therefore critical when targeting a specific design frequency (f_D). The product RCf_D should ideally lie between $1/(2\pi\sqrt{6})$ (approximately 0.065) and $1/(2\pi\sqrt{3})$ (approximately 0.092). To ensure robustness in design, it is preferable to maintain RCf_D within a narrower range of 0.068 to 0.088. This recommended range corresponds to a practically useful region in which the frequency curve remains sufficiently stable for design purposes while the required critical gain remains moderate. Detailed discussions on this aspect are provided in subsequent sections.

2.2 Validation using simulation

It is both valuable and essential to validate our derived formulas by employing modeling packages and simulation software. Figure 4 displays the Simulink model and results based on the block diagram of our oscillator. In this model, the ratio R_i/R is set to 0.5, which results in a critical gain (K_o) value as calculated from Eq. (7), equal to 51. It is observed that when the forward gain ($K = R_f/R_i$) is set slightly below this value ($K = 50.95 \cong 0.999\, K_o$), oscillation does not occur. Conversely, when K exceeds the critical gain ($K = 51.05 \cong 1.001\, K_o$) oscillation begins, and the resultant oscillation frequency (79.549 Hz) is remarkably close to the expected frequency ($f_o = 79.578$ Hz) from Eq. (8).

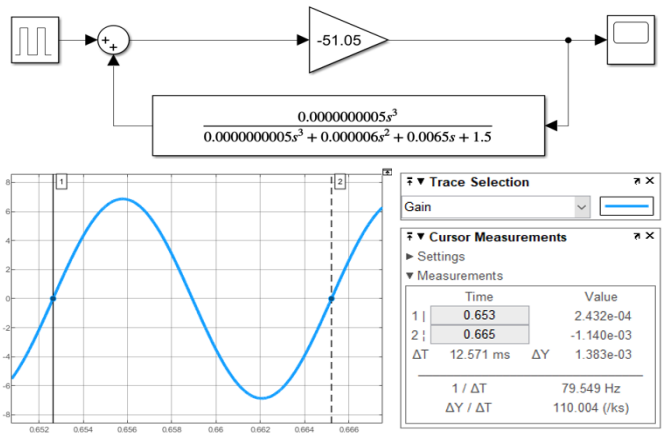

Figure 4. Simulink block representation and modeling results of the oscillator in Figure 2 when the forward gain (K) is set only 0.1% higher than the critical gain (K_o)
Note: The obtained frequency (79.549 Hz) is only 0.036% lower than the theoretical critical frequency.

A similar conclusion is reached through circuit simulations conducted with Multisim, as depicted in Figure 5. In these simulations, ideal op-amp and circuit components are employed, achieving the expected performance both below and above the critical gain with high precision. This consistency confirms the accuracy of the critical condition formulas under ideal conditions.

Ideal conditions are purely theoretical. Therefore, practical validation is also necessary. In the present work, the ideal simulations of Figures 4 and 5 are used only to confirm the correctness of the derived critical-condition formulas. The subsequent practical simulations and measurements employ the LM741 op-amp in order to validate the proposed design methodology under a realistic implementation. This includes the effect of the practical amplifier model used in Multisim and the measured prototype behavior. However, a quantitative study of op-amp non-idealities, such as gain-bandwidth product and slew rate, is beyond the scope of the paper, whose main contribution is the oscillator design process itself.

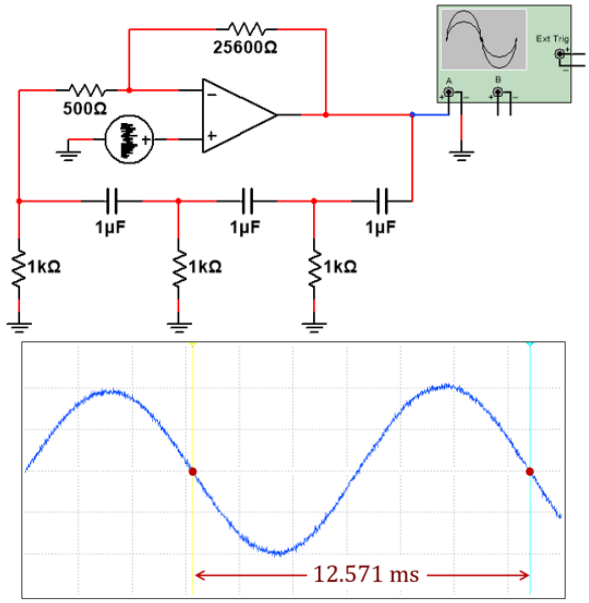

Figure 5. Multisim circuit (top) and simulation results (bottom) of the oscillator in Figure 2, when the forward gain (K) is set only 0.4% higher than the critical gain (K_o)
Note: The obtained frequency (79.548 Hz) is only 0.037% lower than the theoretical critical frequency.

3. TYPICAL DESIGN METHODOLOGY

In what follows, we undertake a realistic design scenario where the entire oscillator circuit is configured to achieve a specific design frequency (f_D) equal to 500 Hz. This design is validated through Multisim simulations using practical components, as well as through subsequent fabrication and measurement. As demonstrated step-by-step, the theoretical formulas serve as a starting point for the design; however, extensive tuning is required to initiate oscillation and to fine-tune the desired oscillation frequency. Moreover, the distortion of the oscillations is considered as an additional design factor. All tuning efforts are conducted via simulations, after which the most optimal design, judged by its frequency accuracy relative to the design goal and minimal distortion, is selected for fabrication and experimental validation.

3.1 Design specifications

The initial objective is to achieve a harmonic oscillation at

precisely $f_D = 500$ Hz. To accomplish this, we will systematically apply the formulas and design curves developed earlier. The design steps are summarized as follows:

Step 1: Select values for R and C such that the product RCf_D ranges from 0.068 to 0.088. This ensures alignment with the oscillation frequency curve shown in Figure 3. Among the available options in our laboratory, we choose $R = 15$ kΩ and $C = 10$ nF, resulting in a RCf_D value of 0.075.

Step 2: Determine the value of R_i either from the critical frequency Eq. (8) or directly from the oscillation critical frequency curve in Figure 3. For our RCf_D value of 0.075, this corresponds to $R_i/R = 1$, or $R_i = R = 15$ kΩ.

Step 3: Calculate the value of R_f using the critical gain Eq. (7) or extract it from the critical gain curve in Figure 3. In our scenario, the $R_i/R = 1$ ratio suggests a critical gain of 39.5, resulting in $R_f = 39.5R_i = 592.5$ kΩ.

With all component values determined, the initial design of the oscillator is complete. To verify the design's functionality, the circuit is assembled in Multisim using the specified components and the LM741 op-amp. However, oscillation was not initiated under this practical implementation. This behavior reflects the presence of practical non-idealities in the circuit and amplifier model, which motivates the tuning study presented next. The purpose here is not to isolate each non-ideality separately, but rather to examine how the conventional design process behaves under practical conditions.

3.2 Tuning approaches

We employed three tuning techniques to activate the oscillator. All techniques are conducted through Multisim simulations using practical components, with subsequent analysis focusing on the oscillation frequency, when present, and the harmonic distortion of the resultant sinusoidal signal. The inclusion of distortion analysis is crucial, as it serves as an indicator of signal purity and can deteriorate due to several factors throughout the tuning process. Identifying these factors is instrumental in refining the design process, as to be presented in the subsequent sections.

The first tuning approach involves solely adjusting the feedback resistor (R_f) to increase the gain above the critical gain threshold. This strategy aims to push the circuit into a state of greater instability, reaching into the shaded region above the critical gain curve depicted in Figure 3. Figure 6 shows the frequency of oscillations obtained in relation to the value of R_f. For each oscillating case, the distortion was evaluated from the exported waveform data using MATLAB-based harmonic analysis. The waveform was first interpolated to a uniform time grid over the steady oscillation interval, and the total harmonic distortion (THD) was then computed using 100 harmonics, with the final value reported in percentage form. This parametric analysis reveals that it is not possible to achieve the necessary oscillation at the targeted design frequency of 500 Hz by varying R_f only. Furthermore, it indicates that the distortion of oscillation worsens (i.e., increasing in magnitude) as R_f is raised. The rationale behind this behavior is explored in the next section, particularly through an examination of the poles of the system's transfer function.

The second tuning approach involves adjusting R_i while maintaining R_f at its theoretically calculated value of 592.5 kΩ. In this strategy, the value of R_i is reduced to increase the gain, thereby increasing instability to ensure the initiation of oscillation. Figure 7 shows the oscillation frequency and distortion as R_i is varied. Achieving the targeted design frequency of 500 Hz is not feasible by tuning R_i alone.

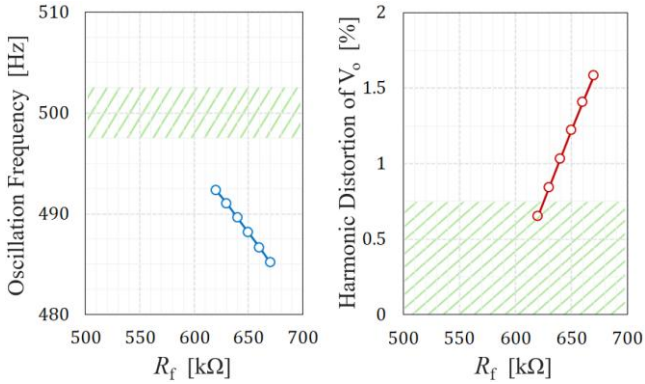

Figure 6. Simulated oscillation frequency (left) and total harmonic distortion (right) of the output signal (V_o) with increased values of R_f

Note: All other component values are fixed at $R_i = R = 15$ kΩ and $C = 10$ nF. Shaded regions represent margins of targeted performance: frequency within ±0.5% of design frequency, and distortion lower than 0.75%. Satisfying both performance aspects simultaneously is not attained.

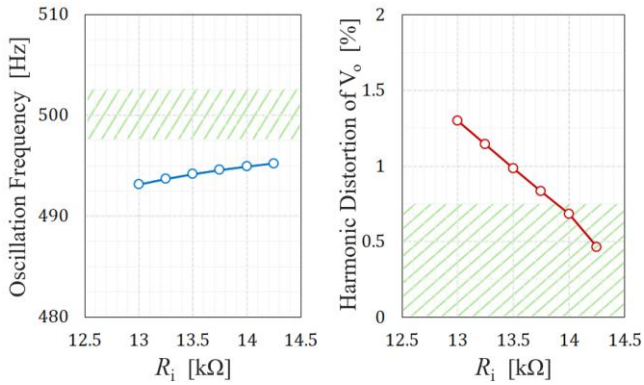

Figure 7. Simulated oscillation frequency (left) and total harmonic distortion (right) of the output signal (V_o) with reduced values of R_i

Note: All other component values are fixed at $R_f = 592.5$ kΩ, $R = 15$ kΩ, and $C = 10$ nF. Shaded regions represent margins of targeted performance: frequency within ±0.5% of design frequency, and distortion lower than 0.75%. Satisfying both performance aspects simultaneously is not attained.

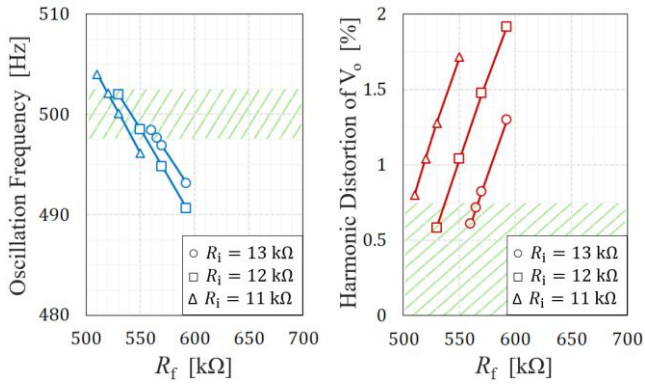

Figure 8. Simulated oscillation frequency (left) and total harmonic distortion (right) of the output signal (V_o) with varying R_i and R_f

Note: All other component values are fixed at $R = 15$ kΩ and $C = 10$ nF. Shaded regions represent margins of targeted performance: frequency within ±0.5% of design frequency, and distortion lower than 0.75%. Satisfying both performance aspects simultaneously is rarely attained (e.g., with $R_i = 12$ kΩ and $R_f = 530$ kΩ).

The third tuning approach entails adjusting both R_{i} and R_{f}. By simultaneously varying these parameters, oscillation at the design frequency of 500 Hz (±0.5%) is achieved, as illustrated in Figure 8. Despite this success, the need to tune two parameters concurrently complicates both the design process and any experimental tuning that might be required during the practical realization stage. However, this method becomes the only viable option, as previous approaches involving the adjustment of a single parameter did not successfully induce oscillation at the desired frequency.

3.3 Experimental validation

A prototype of the 3-stage RC oscillator was realized and tested using the tuned values of R_i and R_f obtained from the tuning study of the previous subsection. The purpose of this experimental stage is to provide practical validation of the proposed design process using available laboratory components and a real op-amp implementation.

Figure 9 shows the circuit schematic, a photograph of the fabricated prototype, and the measured output signal. The fundamental frequency of the obtained oscillation is 498.5 Hz, which is within 0.5% of the target frequency of 500 Hz for this implemented case. The measured total harmonic distortion is 0.79%, as evaluated from the exported waveform data using the same MATLAB-based harmonic analysis procedure with 100 harmonics included in the calculation, which remains low for a 3-stage RC ladder oscillator built with practical components. Minor deviations in the measured behavior may also include contributions from wiring and layout parasitics in the practical prototype, although such effects are secondary at the low frequencies considered here. These results support the practical validity of the proposed methodology under the selected component values. A broader statistical study of component tolerances and yield is left for future work.

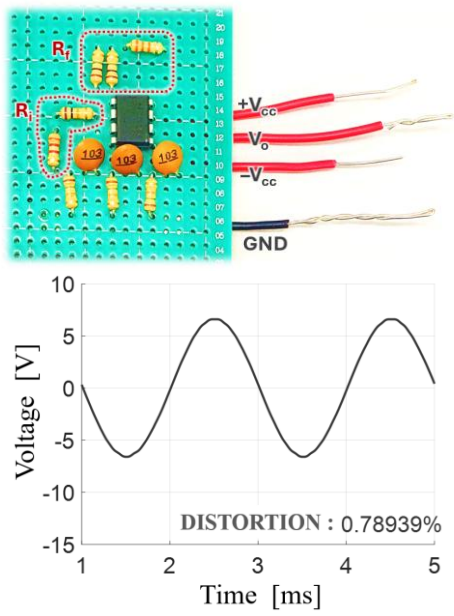

Figure 9. Fabricated oscillator prototype (top) and measured output signal V_{o} (bottom)

Note: The circuit schematic is shown in Figure 2 with the LM741 op-amp and the following component values: $R \approx 15$ kΩ, $C \approx 10$ nF, $R_{\mathrm{i}} \approx 12$ kΩ, $R_{\mathrm{f}} \approx 530$ kΩ. Note that suitable combinations of available in-house resistors are used to obtain R_{i} and R_{f} values. The measured waveform data were exported and processed in MATLAB, yielding a fundamental frequency of 498.5 Hz and a total harmonic distortion of 0.79%.

4. REFINED DESIGN METHODOLOGY

4.1 Practical design aspects

In designing an oscillator circuit, three major aspects are paramount from a practical standpoint:

Design Aspect 1: The circuit should initiate harmonic oscillation without the need for tuning.

Design Aspect 2: The frequency of oscillation should closely match the design frequency, with high precision (within ±0.5%).

Design Aspect 3: Distortion in the obtained harmonic signal should be minimized (less than 0.75%).

A typical design process adheres to the theoretically derived critical gain and frequency formulas, as outlined in Eqs. (7) and (8) for the 3-stage RC oscillator. However, our investigations have shown that these formulas do not reliably predict oscillation initiation in practice, thereby failing to meet Design Aspect 1. Additionally, when tuning is applied to just one parameter (R_{f} or R_{i}) to increase gain and initiate oscillation, the resulting frequency deviates substantially from the design frequency, thereby compromising Design Aspect 2.

One potential solution to this challenge is to initially design the oscillator to operate at a slightly higher frequency than the actual (at 1.05 f_{D}, for instance), then adjust the gain (e.g., by increasing R_{f}) to initiate oscillation and simultaneously reduce the frequency. While this approach may be feasible in practice, it does not offer the precise, predictable outcomes that a purposeful design should provide. Furthermore, if oscillation begins at a frequency higher than intended, further increasing the gain, intended to correct the frequency, will likely increase distortion, thereby compromising Design Aspect 3.

4.2 Practical design curves

In this part, we refine the design process to align with all previously outlined design aspects while maintaining a precise understanding of the circuit's predicted behavior. Instead of solely relying on the critical frequency design curve shown in Figure 3, which is based on the explicit Eq. (8), we develop additional practical design curves at gain values that exceed the critical gain ($K > K_o$). By designing with higher gains from the outset, we ensure compliance with Design Aspect 1, eliminating the need for subsequent tuning that could otherwise shift the oscillation frequency and breach Design Aspect 2. Thus, the inclusion of these additional design curves enhances the robustness of the design framework, facilitating the achievement of the desired performance characteristics with greater ease.

Figure 10 displays the newly developed frequency design curves for forward gain values (K) of K_o, 1.025 K_o, 1.05 K_o, 1.075 K_o, 1.1 K_o, 1.125 K_o, 1.15 K_o, 1.175 K_o, and 1.2 K_o. Each curve is numerically developed by solving the characteristic equation of the oscillator's overall feedback system, as outlined in Eq. (6). For example, assuming $K = 1.025\ K_o$, the critical gain (K_o) is first calculated using Eq. (7) at a specific ratio R_{i}/R. Then, the forward gain K is evaluated at this ratio, and the characteristic equation is solved to identify the roots with positive real parts, indicating instability. The imaginary parts of these roots are extracted to determine the oscillation frequency at that specific R_{i}/R ratio. This procedure is systematically repeated across all R_{i}/R values to complete the design curve for $K = 1.025\ K_o$. The entire process is subsequently replicated to construct the remaining

design curves. For convenient direct use, compact empirical expressions corresponding to these practical frequency curves are provided in Appendix B.

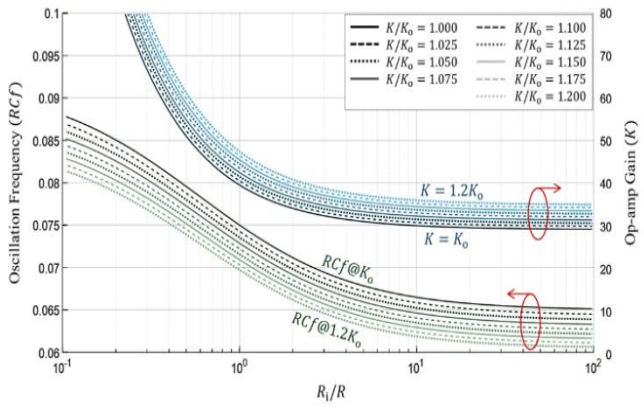

Figure 10. Frequency and gain design curves for a three-stage, single op-amp, Resistor–Capacitor (RC) phase-shift oscillator

Note: These curves are specific to a ladder CR-CR-CR configuration like the circuit in Figure 2. These curves are suited for the practical design methodology outlined in Figure 1.

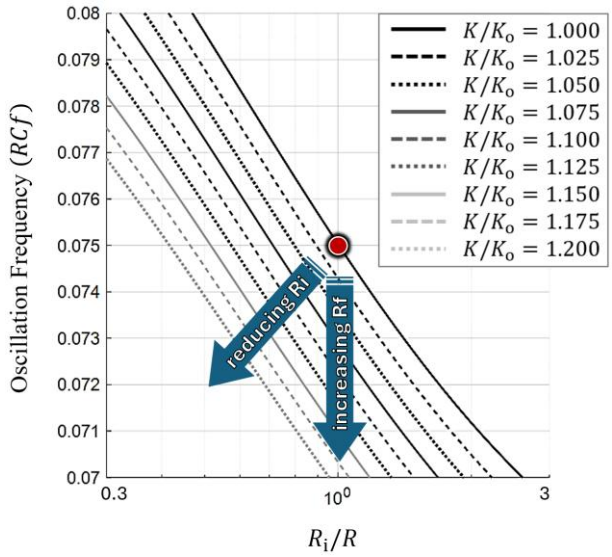

Figure 11. Illustration of the single-parameter tuning approaches

Note: The circle marks the original design point based on typical formulas of critical frequency and critical gain. Tuning by increasing R_f or decreasing R_i triggers the oscillator to initiate, but at a lower frequency, which is confirmed in Figure 6 and Figure 7.

Here is how a designer can effectively use the new curves to design a 3-stage RC oscillator at 500 Hz:

Step 1: Select values for R and C such that the product RCf_D ranges from 0.065 to 0.085. This range has been adjusted downward from 0.068 to 0.088, as used in Section 3.1, to accommodate the use of $K > K_o$ curves. For this design, $R = 15$ kΩ and $C = 10$ nF are chosen, resulting in a RCf_D value of 0.075.

Step 2: Refer to the frequency design curves in Figure 10 to locate the intersection of $RCf_D = 0.075$ and the frequency curve for $K = 1.05\ K_o$. The intersection occurs at $R_i/R = 0.8$, corresponding to $R_i = 0.8R = 12$ kΩ. The obtained value of R_i/R is then used in the analytical critical-gain expression to evaluate K_o, after which the selected gain ratio K/K_o gives the practical gain K, and hence R_f from $K = R_f/R_i$.

Step 3: Refer to the gain design curves of Figure 10 to determine the intersection between $R_i/R = 0.8$ and the gain curve for $K = 1.05\ K_o$. The intersection is found at $K = 44$, corresponding to $R_f = 44R_i = 528$ kΩ.

It is worth noting that the obtained untuned component values ($R_i = 12$ kΩ and $R_f = 528$ kΩ) closely align with the values obtained in Section 3 after extensive tuning. This underscores the robustness of the developed curves for designing oscillators both quickly and precisely, while ensuring proper operation since the design gain is slightly above the critical gain.

The practicality of the developed design curves for making quick adjustments to R_i and R_f values is also noteworthy. For example, if the component values at $K = 1.05\ K_o$ fail to initiate oscillations, switching to a higher gain curve (e.g., $K = 1.075\ K_o$) can provide new component values easily and quickly. Conversely, if lower distortion is desired, recalculating at a lower gain ($K = 1.025\ K_o$) also yields new component values swiftly. Regardless of the design decision, all adjustments can be made with confidence that the oscillation frequency will remain remarkably close to the design frequency of 500 Hz.

4.3 Insights into tuning

Careful examination of Figure 10 may reveal insightful information regarding the oscillator's behavior during tuning. If frequency tuning is performed by increasing R_f alone, the design point transitions from one K curve to a higher K curve (moving downward of the frequency design curves), while the operation point remains constant on the x-axis (since R_i/R is unaffected by changes in R_f). As a result, the obtained oscillation frequency will decrease. Conversely, if tuning involves decreasing R_i alone, the design point shifts from one K curve to a higher K curve (moving downward) and also shifts leftward on the x-axis (since R_i/R decreases with a reduction in R_i). Once again, the obtained oscillation frequency is reduced. Figure 11 illustrates the effect of these tuning approaches on the oscillation frequency. These observations explain why the first and second tuning approaches in Section 3.2 consistently led to reduced frequencies.

From a design perspective, this behavior explains why relying solely on the critical gain and frequency curves (i.e., $K = K_o$) is not practical, as tuning a single parameter (R_f or R_i) will certainly lower the oscillation frequency below the targeted design frequency.

5. DISCUSSION AND GENERALIZATION

5.1 Summary of design process

In our exploration of designing a 3-stage RC oscillator circuit (CR-CR-CR type), we initially utilized control theory to derive the instability conditions necessary to initiate oscillations, where the loading effect is considered when calculating the related transfer functions. More significantly, we have highlighted the practical reasons for designing at a gain higher than the critical gain, and we have documented the oscillator's behavior under such conditions in terms of initiating oscillation and achieving the exact oscillation

frequency. In support of this discussion, we have constructed useful design curves (shown in Figure 10) that allow direct evaluation of all circuit component values that aim to achieve a precise oscillator operation in practice.

Figure 1 presents a flow chart detailing the design process for a practical 3-stage CR-CR-CR type oscillator. Following this methodology allows designers to quickly develop a functioning oscillator whose output harmonic frequency closely matches the intended design frequency. As a quick demonstration, if the target frequency $f_D = 1300$ Hz, we can set $R = 2.4$ kΩ and $C = 22$ nF so that the product $RCf_D = 0.0686$. This product value intersects with the frequency curve of $K = 1.1\,K_o$ at $R_i/R \approx 2$, meaning that $R_i = 4.8$ kΩ. Moving vertically (i.e., maintaining $R_i/R = 2$) yields the intersection with the gain curve of $K = 1.1\,K_o$ at $K \approx 37.5$, meaning that $R_f = 180$ kΩ. This concludes the circuit design, and the Multisim simulation results (not shown here) confirm the accurate oscillation at 1295 Hz (within 0.4% of the target frequency) and a low distortion level of 0.55%. It is important to note that our proposed methodology eliminates the need for any after-design tuning unless a much tighter tolerance of the oscillation frequency is necessary.

5.2 RC-RC-RC ladder type

The methodology presented for developing practical design curves is versatile and can be applied to any RC-ladder oscillator configuration. For example, in a feedback ladder circuit configured as RC-RC-RC, where it starts with a resistor at the op-amp's output and ends with a shunt capacitor at the input, the nodal equations are modified to reflect this arrangement. Nonetheless, the fundamental analysis involving the reduction of transfer functions within the oscillator's feedback control system remains consistent. This analysis leads to the establishment of a critical stability condition for forward gain as follows:

$$K_o = \frac{29\left(\frac{R_i}{R}\right)^2 + 23\frac{R_i}{R} + 4}{\left(\frac{R_i}{R}\right)^2} \tag{9}$$

which corresponds to the following critical frequency:

$$f_o = \frac{1}{2\pi\sqrt{2}RC}\sqrt{\frac{2 + 3\,R_i/R}{R_i/R}} \tag{10}$$

Figure 12 illustrates the critical gain and frequency curves as outlined in Eqs. (9) and (10), along with the practical gain and frequency curves observed when the forward gain ratio (K/K_o) exceeds unity, as typically expected in practice. These design curves prove invaluable when adhering to the design process depicted in Figure 1, with a minor modification: The possible value of the RCf_D product is adjusted to fall within a practical range of (0.4, 0.6). Following this adjusted process, we designed the RC-RC-RC oscillator shown in Figure 13, which operates within 0.5% of the design frequency. This design approach is efficient, proceeding in a step-by-step manner without the need for after-design tuning. The corresponding compact empirical expressions are also included in Appendix B to reduce dependence on graphical estimation during design.

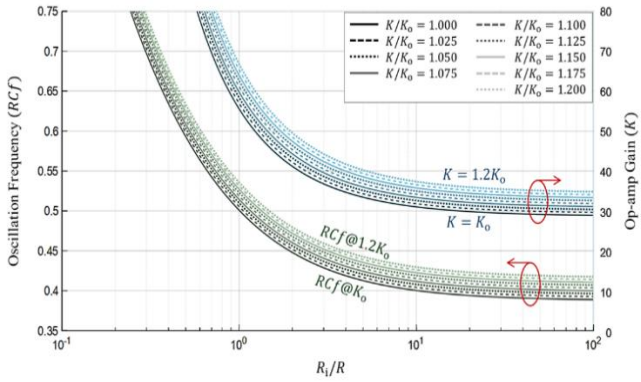

Figure 12. Frequency and gain design curves for a three-stage, single op-amp, Resistor–Capacitor (RC) phase-shift oscillator

Note: These curves are specific to a ladder RC-RC-RC configuration like the circuit in Figure 13.

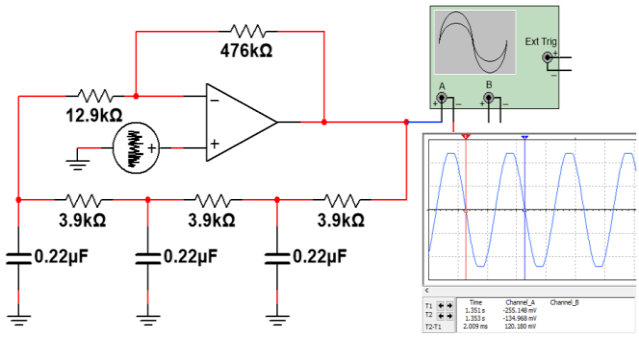

Figure 13. Three-stage, single op-amp, Resistor–Capacitor (RC) phase-shift oscillator with RC-RC-RC ladder configuration

Note: The circuit is designed to produce a 500 Hz oscillator based on the $K \sim K_o$ design curve from Figure 12. No after-design tuning is applied; yet the obtained frequency is very close to the intended design frequency.

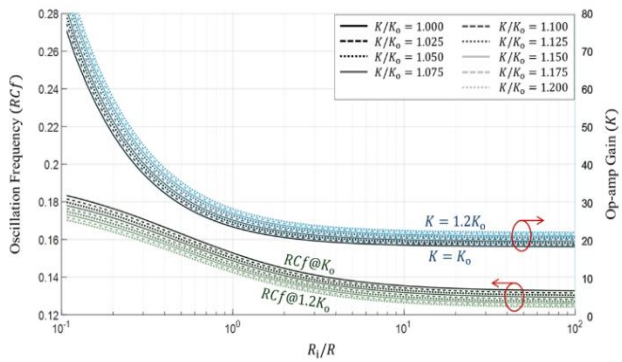

Figure 14. Frequency and gain design curves for a four-stage, single op-amp, Resistor–Capacitor (RC) phase-shift oscillator

Note: These curves are specific to a ladder CR-CR-CR-CR configuration.

5.3 Four-stage oscillators

Further validation of our analysis extends to oscillators with 4-stage RC ladders. Both the CR-CR-CR-CR and RC-RC-RC-RC configurations are explored, and the explicit critical gain and critical oscillation frequency are derived as:

For CR-CR-CR-CR type:

$$K_o = \frac{901\left(\frac{R_i}{R}\right)^3 + 1756\left(\frac{R_i}{R}\right)^2 + 1108\frac{R_i}{R} + 224}{49\left(\frac{R_i}{R}\right)^3 + 84\left(\frac{R_i}{R}\right)^2 + 36\frac{R_i}{R}} \quad (11)$$

$$f_o = \frac{1}{2\pi\sqrt{2}RC}\sqrt{\frac{6 + 7\,R_i/R}{2 + 5\,R_i/R}} \quad (12)$$

For RC-RC-RC-RC type:

$$K_o = \frac{901\left(\frac{R_i}{R}\right)^3 + 1210\left(\frac{R_i}{R}\right)^2 + 473\frac{R_i}{R} + 56}{49\left(\frac{R_i}{R}\right)^3 + 14\left(\frac{R_i}{R}\right)^2 + \frac{R_i}{R}} \quad (13)$$

$$f_o = \frac{\sqrt{10}}{2\pi\,RC}\sqrt{\frac{1 + R_i/R}{1 + 7\,R_i/R}} \quad (14)$$

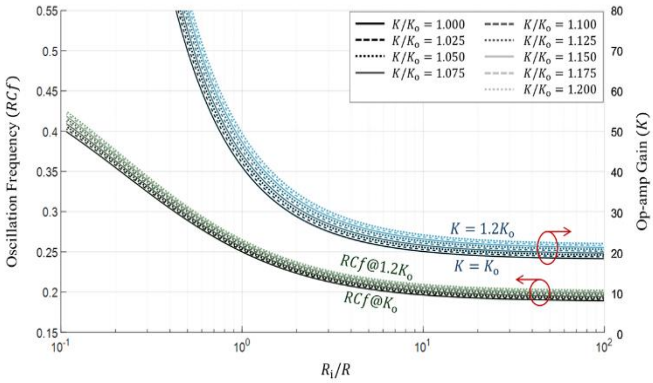

Figure 15. Frequency and gain design curves for a four-stage, single op-amp, Resistor–Capacitor (RC) phase-shift oscillator

Note: These curves are specific to a ladder RC-RC-RC-RC configuration.

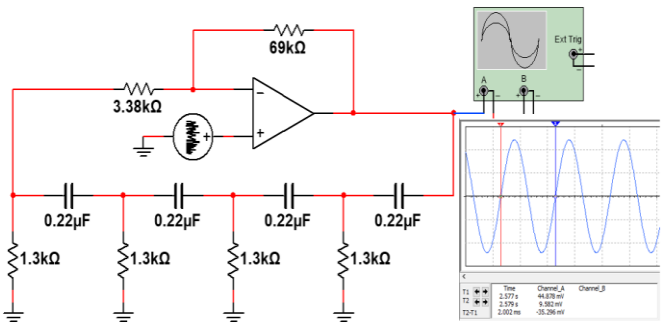

Figure 16. Four-stage, single op-amp, Resistor–Capacitor (RC) phase-shift oscillator with CR-CR-CR-CR ladder configuration

Note: The circuit is designed to produce a 500 Hz oscillator based on the $K \sim K_o$ design curve from Figure 14.

Furthermore, we developed practical gain and frequency design curves for each configuration, which are illustrated in Figures 14 and 15. Employing these curves, we rigorously followed the previously outlined step-by-step process to design two 4-stage RC-ladder oscillators, both operating precisely at 500 Hz, as depicted in Figure 16 and Figure 17. For completeness and direct engineering use, fitted empirical expressions for these practical frequency curves are also provided in Appendix B. The design outcomes were both swift and accurate, eliminating the need for any after-design tuning. Consistent success across different configurations demonstrates the robustness and practicality of the methodology developed in this work.

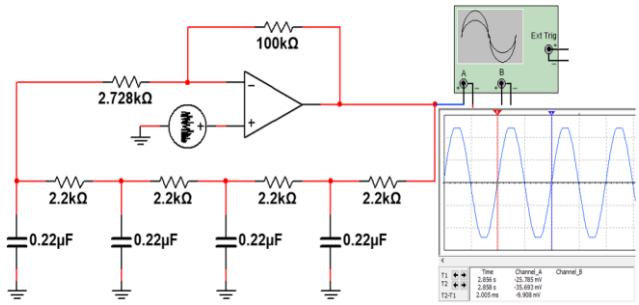

Figure 17. Four-stage, single op-amp, Resistor–Capacitor (RC) phase-shift oscillator with RC-RC-RC-RC ladder configuration

Note: The circuit is designed to produce a 500 Hz oscillator based on the $K \sim K_o$ design curve from Figure 15.

6. CONCLUSION AND FUTURE WORK

We developed a practical design process for single op-amp RC phase-shift oscillators. The method is based on loading-aware transfer-function modeling and accurate characterization beyond the traditional critical stability condition. Since no explicit formulas are available in that operating region, we numerically developed gain-frequency design curves. These curves allow the oscillator to be designed for the required application frequency with high precision, reaching ±0.5% in the demonstrated cases. This level of accuracy, together with the speed of the design process, greatly reduces the need for after-design tuning that is common in conventional approaches. The method was tested through simulations of 3-stage and 4-stage RC phase-shift oscillators and was further confirmed by measurement of a working prototype.

Although this work focused on RC phase-shift oscillators, the same methodology may be extended to other self-starting oscillator topologies that can be modeled through feedback transfer functions. Possible next targets include Wien-bridge oscillators, transistor-based phase-shift oscillators, and other oscillator configurations in which startup occurs above the critical condition. Another useful extension is the application of the method to designs with tunable gain or digitally adjustable components, as well as statistical tolerance analysis for practical implementation.

REFERENCES

[1] Carter, B., Mancini, R. (2017). Op Amps for Everyone. Newnes, Elsevier.

[2] Fuada, S. (2022). Development of educational kit for practical course in the topic of phase-shift RC oscillator. International Journal of Online & Biomedical Engineering, 18(5): 112-130. https://doi.org/10.3991/ijoe.v18i05.29131

[3] Gonzalez, G. (2006). Foundations of Oscillator Circuit Design. Artech, House.

[4] Hajimiri, A., Lee, T.H. (1999). The Design of Low Noise

Oscillators. Springer. https://doi.org/10.1007/b101822
[5] Lepkowski, J. (2003). Designing operational amplifier oscillator circuits for sensor applications. AN866, Microchip Technology Inc., DS00866.
[6] Senani, R., Bhaskar, D.R., Singh, V.K., Sharma, R.K. (2016). Sinusoidal Oscillators and Waveform Generators Using Modern Electronic Circuit Building Blocks. Cham: Springer International Publishing. https://doi.org/10.1007/978-3-319-23712-1
[7] Westra, J.R., Verhoeven, C.J.M., van Roermund, A.H.M. (1999). Oscillators and Oscillator Systems: Classification, Analysis and Synthesis. Kluwer Academic Publishers, Boston, MA, USA. https://doi.org/10.1007/978-1-4757-6117-7
[8] Ahmed, H.B., Saleh, A.H., Humood, K.A., Mahmood, T. (2024). Design Wien bridge oscillator for VLF to VHF using practical Op–Amp. International Journal of Electrical and Electronics Research, 12(3): 727-733. https://doi.org/10.37391/IJEER.120301
[9] Pang, K. (1969). Chebyshev rational functions and ladder RC networks. IEEE Transactions on Circuit Theory, 16(3): 408-410. https://doi.org/10.1109/TCT.1969.1082987
[10] Pang, K. (1971). Optimum RC phase-shift network between two arbitrary impedances. IEEE Transactions on Circuit Theory, 18(2): 255-259. https://doi.org/10.1109/TCT.1971.1083250
[11] Fano, R.M. (1950). Theoretical limitations on the broadband matching of arbitrary impedances. Journal of the Franklin Institute, 249(1): 57-83. https://doi.org/10.1016/0016-0032(50)90006-8
[12] Youla, D. (2003). A new theory of broad-band matching. IEEE Transactions on Circuit Theory, 11(1): 30-50. https://doi.org/10.1109/TCT.1964.1082267
[13] Sulzer, P.G. (2006). The tapered phase-shift oscillator. Proceedings of the IRE, 36(10): 1302-1305. https://doi.org/10.1109/JRPROC.1948.231940
[14] Ogorzalek, M.J. (1989). Order and chaos in a third-order RC ladder network with nonlinear feedback. IEEE Transactions on Circuits and Systems, 36(9): 1221-1230. https://doi.org/10.1109/31.34668
[15] Wang, J., Adhikari, G., Tsukiji, N., Kobayashi, H. (2018). Analysis and design of operational amplifier stability based on Routh-Hurwitz stability criterion. IEEJ Transactions on Electronics, Information and Systems, 138(12): 1517-1528. https://doi.org/10.1541/ieejeiss.138.1517
[16] Rochelle, J. (1969). An approximation for transfer functions having only infinite zeros and negative real poles. IEEE Transactions on Circuit Theory, 16(3): 410-411. https://doi.org/10.1109/TCT.1969.1082988
[17] Sherr, S. (1954). Generalized equations for RC phase-shift oscillators. Proceedings of the IRE, 42(7): 1169-1172. https://doi.org/10.1109/JRPROC.1954.274552
[18] Lewis, E. (1974). A note on transfer and driving-point functions of iterated ladder networks. IEEE Transactions on Circuits and Systems, 21(3): 334-338. https://doi.org/10.1109/TCS.1974.1083869
[19] Singh, V. (2007). Failure of Barkhausen oscillation building up criterion: Further evidence. Analog Integrated Circuits and Signal Processing, 50(2): 127-132. https://doi.org/10.1007/s10470-006-9008-6
[20] Singh, V. (2010). Discussion on Barkhausen and Nyquist stability criteria. Analog Integrated Circuits and Signal Processing, 62(3): 327-332. https://doi.org/10.1007/s10470-009-9360-4
[21] von Wangenheim, L. (2011). On the Barkhausen and Nyquist stability criteria. Analog Integrated Circuits and Signal Processing, 66(1): 139-141. https://doi.org/10.1007/s10470-010-9506-4
[22] Martínez-García, H., Grau-Saldes, A., Bolea-Monte, Y., Gámiz-Caro, J. (2012). On 'Discussion on Barkhausen and Nyquist stability criteria'. Analog Integrated Circuits and Signal Processing, 70(3): 443-449. https://doi.org/10.1007/s10470-011-9730-6
[23] Abuelma'atti, M.T., Khalifa, Z.J. (2012). Comment on 'Discussion on Barkhausen and Nyquist stability criteria'. Analog Integrated Circuits and Signal Processing, 73(3): 989-992. https://doi.org/10.1007/s10470-012-9907-7
[24] He, F., Ribas, R., Lahuec, C., Jézéquel, M. (2009). Discussion on the general oscillation startup condition and the Barkhausen criterion. Analog Integrated Circuits and Signal Processing, 59(2): 215-221. https://doi.org/10.1007/s10470-008-9250-1
[25] Lin, C.W., Chen, Y.T., Chen, Y.C., Chen, C.C. (2017). Improvement of the Barkhausen criterion and the implementation of an intelligent function generator. The Journal of Engineering, 2017(4): 126-138. https://doi.org/10.1049/joe.2017.0021
[26] Jiang, W.M., Chen, C.C., Chen, Y.T., Wang, J.C. (2021). New method of solving the oscillation criterion for Hartley oscillator. Iranian Journal of Science and Technology, Transactions of Electrical Engineering, 45(4): 1117-1125. https://doi.org/10.1007/s40998-021-00432-x
[27] Georgiev, Z.D., Uzunov, I.M., Todorov, T.G., Trushev, I.M. (2024). The Poincaré-Andronov-Hopf bifurcation theory and its application to nonlinear analysis of RC phase-shift oscillator. International Journal of Circuit Theory and Applications, 52(3): 1399-1437. https://doi.org/10.1002/cta.3783
[28] Maundy, B.J., Elwakil, A.S., Elamien, M.B., Psychalinos, C. (2025). Review and novel contributions to amplifier-based oscillator design. AEU - International Journal of Electronics and Communications, 190: 155633. https://doi.org/10.1016/j.aeue.2024.155633
[29] Maundy, B.J., Elwakil, A.S., Psychalinos, C. (2023). Systematic realization of tunable-phase third-order oscillators. AEU - International Journal of Electronics and Communications, 170: 154806. https://doi.org/10.1016/j.aeue.2023.154806
[30] Bhaskar, D.R., Raj, A., Senani, R. (2023). Third-order quadrature sinusoidal oscillators with fully uncoupled tuning laws using only two CFOAs and grounded capacitors. International Journal of Circuit Theory and Applications, 51(6): 2981-2992. https://doi.org/10.1002/cta.3567
[31] Senani, R., Bhaskar, D.R., Gupta, S.S., Sharma, R.K. (2023). An ingenious methodology of deriving single-FTFN-based canonic grounded-capacitor SRCOs. International Journal of Circuit Theory and Applications, 51(4): 1918-1934. https://doi.org/10.1002/cta.3501

NOMENCLATURE

C	Capacitance, Farads

f	Frequency, s^{-1} or Hz
G	Op-amp forward-path gain, dimensionless
K	Gain absolute value, dimensionless
H	Feedback transfer function, dimensionless
R	Resistance, Ohms [Ω]
V	Voltage, Volts [V]
THD	Total harmonic distortion, %

Greek symbols

π	Pi constant

Subscripts

i	Input, such as in R_i
out	Output, such as in V_{out}
D	Design or target, such as in f_D
o	Critical condition, such as in K_o
f	Feedback, such as in V_f

APPENDIX

Appendix A. Derivation of the critical-gain expression using the Routh-Hurwitz criterion

Starting from the characteristic equation in Eq. (6),

$$(1+K)C^3R^3\frac{R_\mathrm{i}}{R}s^3+\left(3+6\frac{R_\mathrm{i}}{R}\right)C^2R^2s^2 + \left(4+5\frac{R_\mathrm{i}}{R}\right)CRs+\left(\frac{R_\mathrm{i}}{R}+1\right)=0 \tag{A1}$$

let:

$$x=\frac{R_i}{R} \tag{A2}$$

Eq. (A1) can then be written in the standard cubic form:

$$a_3s^3+a_2s^2+a_1s+a_0=0 \tag{A3}$$

with coefficients:

$$a_3=(1+K)C^3R^3x \tag{A4}$$

$$a_2=(3+6x)C^2R^2 \tag{A5}$$

$$a_1=(4+5x)CR \tag{A6}$$

$$a_0=x+1 \tag{A7}$$

For a third-order characteristic polynomial, the Routh-Hurwitz array is:

$$\begin{array}{lcc} s^3 & a_3 & a_1 \\ s^2 & a_2 & a_0 \\ s^1 & \dfrac{a_2a_1-a_3a_0}{a_2} & 0 \\ s^0 & a_0 & \end{array} \tag{A8}$$

At critical stability, the first element of the s^1 row becomes zero. Therefore, the oscillation boundary is obtained from:

$$a_2a_1-a_3a_0=0 \tag{A9}$$

Substituting Eqs. (A4)–(A7) into Eq. (A9) gives:

$$(3+6x)(4+5x)C^3R^3=(1+K)x(x+1)C^3R^3 \tag{A10}$$

which simplifies to:

$$(3+6x)(4+5x)=(1+K)x(x+1) \tag{A11}$$

Solving for K yields the critical gain:

$$K_o=\frac{29x^2+38x+12}{x^2+x} \tag{A12}$$

or equivalently:

$$K_o=\frac{29\left(\frac{R_i}{R}\right)^2+38\left(\frac{R_i}{R}\right)+12}{\left(\frac{R_i}{R}\right)^2+\left(\frac{R_i}{R}\right)} \tag{A13}$$

which is the expression reported in Eq. (7).

To obtain the critical oscillation frequency, the auxiliary equation is taken from the s^2 row of the Routh table:

$$a_2s^2+a_0=0 \tag{A14}$$

Substituting Eqs. (A5) and (A7) gives:

$$(3+6x)C^2R^2s^2+(x+1)=0 \tag{A15}$$

Hence, under critical conditions:

$$\omega_o=\frac{1}{CR}\sqrt{\frac{x+1}{6x+3}} \tag{A16}$$

and therefore:

$$f_o=\frac{1}{2\pi CR}\sqrt{\frac{x+1}{6x+3}} \tag{A17}$$

or, in terms of R_i/R:

$$f_o=\frac{1}{2\pi RC}\sqrt{\frac{\left(\frac{R_i}{R}\right)+1}{6\left(\frac{R_i}{R}\right)+3}} \tag{A18}$$

which is the critical-frequency expression reported in Eq. (8).

Appendix B. Empirical design formulas for the practical frequency curves

The practical frequency curves shown in Figures 10, 12, 14, and 15 were developed to support direct oscillator design at gain levels slightly above the critical condition. To improve their engineering usability, compact empirical formulas were obtained for all four configurations. They allow the designer to bypass manual reading of the practical frequency curves. Once R, C, and the intended gain ratio α are selected, the

appropriate configuration-specific form of (B1) can be used to determine R_i/R, and hence R_i. The final gain K is then evaluated from the exact relation $K = \alpha K_o$, where K_o is calculated from the original analytical critical-gain expression of the corresponding oscillator configuration. The resistor R_f is then obtained from $K = R_f/R_i$.

B.1 Unified design usage

For all oscillator configurations considered in this work, the design sequence is as follows:

1. Select R and C first based on the required oscillation frequency, so that the normalized quantity RCf is known.
2. Choose a gain ratio $\alpha = \frac{K}{K_o}$ within the practical range $1 \le \alpha \le 1.2$ to ensure oscillation startup under practical conditions.
3. Use the empirical formula corresponding to the selected ladder configuration to evaluate the ratio R_i/R.
4. Determine R_i from the obtained ratio R_i/R, since R is already known.
5. Evaluate the critical gain K_o from the original analytical formula of the corresponding configuration.
6. Compute the practical gain from $K = \alpha K_o$.
7. Since $K = \frac{R_f}{R_i}$ the feedback resistor R_f can then be obtained directly.

Accordingly, the empirical formulas in this appendix serve only to estimate R_i/R from known values of RCf and α, while the gain value K is still determined from the original analytical critical-gain expression.

B.2 General fitting form

For all four configurations, the ratio R_i/R was approximated using the same rational form:

$$\frac{R_i}{R} \approx \frac{p_1(\alpha)(RCf)^2 + p_2(\alpha)(RCf) + p_3(\alpha)}{RCf + q_1(\alpha)} \tag{B1}$$

where, $\alpha = K/K_o$. For each configuration, the four coefficient functions $p_1(\alpha)$, $p_2(\alpha)$, $p_3(\alpha)$, and $q_1(\alpha)$ were found to be well approximated by linear expressions in α.

B.3 Three-stage CR-CR-CR configuration

For the practical frequency curves of Figure 10, the fitted coefficient functions are:

$$p_1(\alpha) = 0.34923\alpha + 0.45900 \tag{B2}$$

$$p_2(\alpha) = -0.036957\alpha - 0.692543 \tag{B3}$$

$$p_3(\alpha) = -0.019316\alpha + 0.079473 \tag{B4}$$

$$q_1(\alpha) = 0.022413\alpha - 0.087307 \tag{B5}$$

These linear fits achieved R^2 values of 0.99957, 0.99749, 0.99901, and 0.99884 for p_1, p_2, p_3, and q_1, respectively.

B.4 Three-stage RC-RC-RC configuration

For the practical frequency curves of Figure 12, the fitted coefficient functions are:

$$p_1(\alpha) = -0.04118\alpha + 0.106799 \tag{B6}$$

$$p_2(\alpha) = 0.055781\alpha - 0.261661 \tag{B7}$$

$$p_3(\alpha) = 0.035622\alpha + 0.164658 \tag{B8}$$

$$q_1(\alpha) = -0.14218\alpha - 0.24794 \tag{B9}$$

These linear fits achieved R^2 values of 0.99764, 0.99828, 0.99983, and 0.99966 for p_1, p_2, p_3, and q_1, respectively.

B.5 Four-stage CR-CR-CR-CR configuration

For the practical frequency curves of Figure 14, the fitted coefficient functions are:

$$p_1(\alpha) = 0.20997\alpha + 0.14601 \tag{B10}$$

$$p_2(\alpha) = -0.063399\alpha - 0.545251 \tag{B11}$$

$$p_3(\alpha) = -0.028708\alpha + 0.133768 \tag{B12}$$

$$q_1(\alpha) = 0.042734\alpha - 0.175754 \tag{B13}$$

These linear fits achieved R^2 values of 0.99946, 0.99773, 0.99934, and 0.99900 for p_1, p_2, p_3, and q_1, respectively.

B.6 Four-stage RC-RC-RC-RC configuration

For the practical frequency curves of Figure 15, the fitted coefficient functions are:

$$p_1(\alpha) = -0.12573\alpha + 0.46424 \tag{B14}$$

$$p_2(\alpha) = 0.075941\alpha - 0.555381 \tag{B15}$$

$$p_3(\alpha) = 0.021885\alpha + 0.138655 \tag{B16}$$

$$q_1(\alpha) = -0.063322\alpha - 0.127048 \tag{B17}$$

These linear fits achieved R^2 values of 0.99816, 0.99836, 0.99971, and 0.99955 for p_1, p_2, p_3, and q_1, respectively.